BBA - Molecular and Cell Biology of Lipids 1870 (2025) 159657

Contents lists available at ScienceDirect

BBA - Molecular and Cell Biology of Lipids

journal homepage: www.elsevier.com/locate/bbalip

LIMP-2 deficiency-associated glycolipid abnormalities in mice

Paulo Gaspar [a,b,c,1], André R.A. Marques [a,2], Maria J. Ferraz [a,d], Markus Damme [e], Gertjan Kramer [a], Mina Mirzaian [d], Marion Gijbels [a], Roelof Ottenhoff [a], Cindy van Roomen [a], Herman S. Overkleeft [f], Michael Schwake [g], Saskia Heybrock [e], Maria Carmo Macário [h], Paul Saftig [e], Johannes M. Aerts [a,d,*]

[a] Department of Medical Biochemistry, Academic Medical Center, Amsterdam, the Netherlands
[b] Organelle Biogenesis & Function Group, Instituto de Investigação e Inovação em Saúde and Institute of Molecular and Cell Biology, Universidade do Porto, Porto, Portugal
[c] Instituto de Ciências Biomédicas Abel Salazar, Universidade do Porto, Porto, Portugal
[d] Department of Medical Biochemistry, Leiden Institute of Chemistry, Leiden University, the Netherlands
[e] Department of Biochemistry, Christian-Albrecht-University of Kiel, Kiel, Germany
[f] Department of Bio-organic Synthesis, Leiden Institute of Chemistry, Leiden University, the Netherlands
[g] Department of Chemistry, Biochemistry III, Bielefeld, Germany
[h] Neurology Department, Coimbra Hospital and University Center, Coimbra, Portugal

ARTICLE INFO

Keywords:
Cerebrosides
Cholesterol
Gaucher's disease
Mass spectrometry
LIMP-2
Glucocerebrosidase
Lysosomes
Glucosylceramide
Glucosylcholesterol
SCARB2
GBA

ABSTRACT

Glucocerebrosidase (GCase) catalyzes the lysosomal degradation of glucosylceramide (GlcCer). GCase deficiency results in Gaucher disease (GD), a lysosomal storage disorder with characteristic hepatosplenomegaly. Transport of GCase to lysosomes is mediated by the lysosomal integral membrane protein type 2 (LIMP-2). Deficiency of LIMP-2 leads to reduced cellular GCase levels and manifests as Action Myoclonic Renal Failure Syndrome (AMRF). We investigated the cause for the markedly different symptomatology of GD and AMRF. In tissues of *Limp2* −/− mice no prominent abnormalities in lysosomal enzymes were noted except for variable deficiency of GCase, as measured with enzymatic activity assay and detection of active GCase molecules with an activity-based probe. Noteworthy, in LIMP-2-deficient mice, residual GCase is remarkably high in leukocytes. GCase deficiency in tissues does not correlate with increases in GlcCer, but rather with increases in glucosylsphingosine (GlcSph) and glucosylated cholesterol (GlcChol), both glucosylated metabolites derived from GlcCer. Isolated lysosomes from hepatocytes of *Limp2* −/− mice revealed no prominent abnormalities in lysosomal matrix proteins except GCase. The *Limp2* −/− tritosomes showed clear increases in GlcSph and GlcChol but not in GlcCer. In conclusion, our data imply a critical role of LIMP-2 in glycosphingolipid homeostasis. Despite low GCase levels striking GlcCer accumulation is avoided in tissues of LIMP-2 deficient mice.

1. Introduction

Gaucher disease (GD) is caused by primary defects in glucocerebrosidase (GCase), the lysosomal β-glucosidase responsible for degradation of glucosylceramide (GlcCer) [1]. In the most common variant without central nervous system (CNS) involvement (type 1), GD manifests as a macrophage disorder with characteristic hepatosplenomegaly, skeletal deterioration and pancytopenia [1]. The lysosomal integral membrane protein type 2 (LIMP-2) encoded by *SCARB2* has been shown to mediate transport and stabilization of newly formed GCase to lysosomes [2–4]. Furthermore, LIMP-2 plays a role in lysosome biogenesis [5], binds the adhesive glycoprotein thrombospondin-1 [6], and assists cell entry by viruses like coxsackievirus A16 and enterovirus [7–9]. Mutations in the *SCARB2* gene cause Action Myoclonic Renal Failure Syndrome (AMRF), a rare form of progressive myoclonic epilepsy (PME)

* Corresponding author at: Department of Medical Biochemistry, room DE.1.19, Leiden Institute of Chemistry, Leiden University, Einsteinweg 55, 2333 CC Leiden, the Netherlands.
E-mail address: j.m.f.g.aerts@lic.leidenuniv.nl (J.M. Aerts).
[1] Present address: Newborn Screening, Metabolism & Genetics Unit, Human Genetics Department, National Institute of Health Doutor Ricardo Jorge, Porto, Portugal.
[2] Present address: iNOVA4Health, NOVA Medical School | Faculdade de Ciências Médicas, NMS|FCM, Universidade Nova de Lisboa, Lisboa, Portugal.

https://doi.org/10.1016/j.bbalip.2025.159657
Received 8 April 2025; Received in revised form 28 June 2025; Accepted 29 June 2025
Available online 8 July 2025

Abbreviations

4-MU-β-d-Glc	4-Methylumbelliferyl-β-d-glucopyranoside
ABP	activity based probe
AF	Abdominal fat
AG	Adrenal gland
AMRF	action myoclonic renal failure syndrome
BAT	Brown adipose tissue
BM	Bone marrow
CCL18	C-C Motif Chemokine Ligand 18
Cer	Ceramide
CNS	Central Nervous System
EF	Epidydimal fat
EP	Epididymis
Gb3	globotriosylceramide
GCase	glucocerebrosidase
GalCer	galactosylceramide
GlcCer	glucosylceramide
GD	Gaucher disease
GlcChol	glucosylated cholesterol
GlcSph	glucosylsphingosine
HexCer	Hexosylceramide
HexSph	hexosylsphingosine
IF	Inguinal fat
LacCer	Lactosylceramide
LC-MS	Liquid chromatography–mass spectrometry
LPH	lactase-phlorizin hydrolase
LIMP-2	lysosomal integral membrane protein type 2
LN	Lymph node
LysoGb3	Globotriaosylsphingosine
OF	Omental fat
OPA	0-phthaldialdehyde
PBMC	peripheral blood mononuclear cells
PBS	Phosphate Buffered Saline
PCR	Polymerase Chain reaction
PME	Progressive myoclonic epilepsy
SCDase	sphingolipid ceramide n-deacylase
SDS_PAGE	Sodium Dodecyl Sulfate-Polyacrylamide Gel Electrophoresis
SG	Salivary gland
SN	Sciatic nerve
SPE	Solid phase extraction
TBS	tris-buffered saline
TE	Testis

[3,10–18]. This disease is associated with proteinuria, kidney failure, collapsing focal and segmental glomerular sclerosis and neurological symptoms including PME and ataxia, but without cognitive decline [2,14,19]. A number of AMRF patients have been reported with disease restricted to the neurological system [10,11,15,16,20]. LIMP-2, belonging to the CD36 superfamily, is an abundant lysosomal membrane protein [21]. It is a type III membrane glycoprotein that transverses the membrane twice with a large luminal domain and a second membrane-spanning domain preceding a 20 amino acid cytoplasmic tail at the C-terminus. A leucine-isoleucine motif within the C-terminal cytoplasmic tail of LIMP-2 mediates lysosomal localization [22–24]. In the endoplasmic reticulum, LIMP-2 binds through its triple helical structure in the apical region (aa 152–167) to the correctly folded GCase [25–28]. The complex of LIMP-2 and GCase is transported from the endoplasmic reticulum to acidic (pre)lysosomal compartments where dissociation occurs [28,29]. Absence of functional LIMP-2 abolishes normal routing of GCase to lysosomes [2]. The small fraction of enzyme that manages to pass the endoplasmic reticulum in the absence of LIMP-2 is thought to be secreted to the extracellular space [30]. No prominent lipid storage is observed in macrophages of AMRF patients [3,14]. Circulating markers of lipid-laden macrophages in GD patients, like chitotriosidase and C-C Motif Chemokine Ligand 18 (CCL18) [31] are normal in AMRF patients [3,14]. The luminal (intralysosomal) domain of LIMP-2 [25] contains a hydrophobic tunnel that transverses the entire domain. Cholesterol and phosphatidylcholine molecules were found in this tunnel [32]. A role of LIMP-2 in transporting cholesterol out of the lysosomal lumen to the lysosomal membrane is supported by molecular modeling and cell-based assays [33]. The transported cholesterol can then be delivered to lipid droplets forming at the ER, likely through transient membrane contacts between lysosomal and ER membranes [34]. Recent studies have provided significant insights into the structure and interaction GCase and LIMP-2. LIMP-2 acts as an allosteric activator of GCase, with potential therapeutic implications [35]. Furthermore, small molecule modulators can promote GCase dimerization and reveal an allosteric binding site, offering new avenues for drug development [36]. In a recent paper by Rudnik et al. evidence is presented for interaction of LIMP-2 with the endosomal protein STARD3 and the ER-resident protein VAPB [37]. These findings collectively enhance our understanding of GCase-LIMP-2 interactions and provide potential strategies for treating Gaucher's disease and Parkinson's disease through GCase activation and stabilization [38,39].

Studies on the deficiency of GCase in AMRF and its consequences at lipid metabolite level are hampered by the scarcity of patients for investigation. Fortunately, a genuine animal model for AMRF was generated some years ago by producing a knock-out of the *SCARB2* gene in mice [40]. The disease symptoms of these *Limp2* −/− mice phenotypically resemble AMRF in man in many aspects, e.g. neuronal accumulation and sclerosis of glomeruli [19]. These animals allow a detailed investigation of the biochemical consequences of the absence of LIMP-2. We examined both GCase and its lipid metabolites in a wide set of tissues of *Limp2* −/− mice. In our analysis of GCase we employed measurement of enzymatic activity as well as labeling with a fluorescent activity-based probe that specifically labels active GCase molecules through covalent binding to the catalytic nucleophile residue [30,41,42]. Next to GlcCer, the primary substrate of GCase, we also analyzed its deacylated form, glucosylsphingosine (GlcSph), known to be generated by lysosomal acid ceramidase and to be markedly increased in tissues as well as plasma of GD patients [31,43,44]. A newly recognized abnormal metabolite in GD patients, glucosylated cholesterol (GlcChol) [45], was also examined. Here, we report the outcome of our research.

2. Materials & methods

2.1. Animal studies

All animal protocols were approved by the Institutional Animal Welfare Committee of the Academic Medical Center Amsterdam in the Netherlands (DBC17AE). The generation of *Limp2* −/− mice was described earlier [40]. Homozygous wild type (*wt*) animals (*Limp2* +/+) and homozygous affected animals (*Limp2* −/−) were obtained by crossing heterozygous (*Limp2* +/−) mice. Genotype was determined by Polymerase Chain Reaction (PCR) using genomic DNA isolated from a small piece of the ear. The mice were housed at the Institute Animal Core Facility in a temperature- and humidity-controlled room with a 12-h light/dark cycle and given free access to food and water ad libitum. A total of 48 animals were used, equally distributed by age (2, 4, 6 and 12 months). Each age had 12 animals (6 *wt*; 6 *Limp2* −/−), uniformly divided by sex (3 male, 3 female).

2.2. Tissue collection

Animals were anesthetized with a dose of Hypnorm (0.315 mg/mL fentanyl citrate and 10 mg/mL fluanisone) and Dormicum (5 mg/mL midazolam) according to their weight. The given dose was 80 μL/10 g body weight. The animals were sacrificed by cervical dislocation. Blood was collected by heart puncture into EDTA tubes and used for lipid measurements. Tissues and organs were collected by surgery and rinsed with phosphate buffered saline (PBS). Each one was sliced in half: one half was directly snap-frozen in liquid nitrogen and stored at −80 °C and the other half was conserved in 10 % (*v*/v) formaldehyde for posterior pathology analysis. Bile was collected for 15 min via cannulation of the gall bladder. Urine was collected through the aspiration of the bladder. Bone marrow was extracted from the hind legs. The skin and flesh were removed, to expose the tibia and femur. Both ends of the collected femur were excised and bone marrow was removed by rinsing with ice cold PBS and the fluid was collected in a 50 mL tube. The cells in the aspirate were centrifuged for 10 min at 2500 rpm (4 °C). The supernatant was discarded, and the pellet was washed again. The pellet was taken up in 1 mL ice cold PBS, transferred to a 1.5 mL Eppendorf tube and centrifuged for 5 min at 13200 rpm (4 °C). The supernatant was discarded and the pellet stored at −80 °C.

2.3. Plasma and leukocytes

Blood collected in EDTA tubes was centrifuged for 10 min at 4000 rpm. Plasma was collected in an Eppendorf tube and stored at −80 °C. The leukocyte layer was transferred to a 50 mL tube with 45 mL of erythrocyte lysis buffer (NH_4Cl/EDTA buffer, pH 7.4). After 20 min shaking at 4 °C on a roller mixer, the tube was centrifuged at 2500 rpm for 10 min (4 °C). The supernatant was discarded and 45 mL of lysis buffer was added. This procedure was repeated to remove all erythrocytes. The pellet was then resuspended in 1 mL ice cold PBS and transferred to a 1.5 mL Eppendorf tube and centrifuged for 5 min at 13200 rpm (4 °C). The supernatant was discarded and the leukocyte pellet was stored at −80 °C.

2.4. Tissue homogenization

Homogenization procedures were performed with RNAse-free glass beads in 2 mL screwcap Eppendorf tubes. 25 mM potassium phosphate buffer (pH 6.5), containing 0.1 % (*v*/v) Triton X-100 and protease inhibitor cocktail (Roche) was added to tissue in a 1:5 ratio. Samples were homogenized with a Tissue Lyser FastPrep®-24 (M. P. Biomedicals, Irvine, CA, USA) set 6 ms^{-1} for 30 s. Homogenates were cooled for 1 min on ice between runs. Smaller tissues (eye, salivary gland, sciatic nerve, lymph node, epididymis and adrenal gland) were homogenized by sonication (40 % power, 40 % amplitude for 6 s) using the sonicator Vibra Cell™ Model no. CV18 (Sonics, Danburry, CT, USA). In the case of leukocyte and bone marrow preparations, 100 μL of the same extraction buffer was added to the pellets and these were homogenized by sonication as described above. All homogenates were stored at −80 °C.

2.5. Protein measurement with the Bicinchoninic acid (BCA™) assay

For quantification of protein the Pierce™ BCA Protein Assay Kit (Pierce Biotechnology Inc., No. 23225) was used according to the manufacturer's protocol.

2.6. Isolation of lysosomes

Lysosomes were purified as follows. Briefly, mice were treated by a single injection of 0.75 mg of tyloxapol (Triton WR1339 Sigma) per g of body weight, 4 days prior to liver collection. This treatment leads to the accumulation of the non-digestible Triton WR 1339 in lysosomes of hepatocytes. Four days after the tyloxapol administration, animals were sacrificed and the livers collected. Cells were gently disrupted leaving lysosomes intact. The density of tyloxapol-laden lysosomes (tritosomes) is below 1 g/mL, facilitating their separation from other cell organelles. The isolation of tritosomes from tyloxapol-treated mice included differential centrifugation and isopycnic centrifugation and resulted in a lysosome-enriched fraction as described earlier [46].

2.7. LC-MS/MS proteomics

Proteins were denatured by heating at 95 °C for 15 min, followed by reduction of disulfide bridges with 5 mM DTT 30 min at 60 °C and alkylation for 30 min with 15 mM iodoacetamide ambient temperature in the dark. Trypsinization was carried out overnight at 37 °C (1:25 *w*/w trypsin ratio). Finally, RapiGest detergent was removed by acidifying digest to pH 2 with trifluoroacetic acid and incubation for 15 min at 37 °C followed by centrifugation at 10000 *g* for 10 min and transfer of the supernatant to a clean tube. Nanoscale LC separation of the tryptic peptides was performed with a NanoAcquity system coupled to a Synapt G2 Q-TOF (quadrupole time-of-flight) mass spectrometer (Waters) operated in data independent, alternate scanning (LC-MSE) mode of acquisition as described before [47,50]. Continuum LC-MS data were processed and searched using ProteinLynx GlobalSERVER v2.5 (Waters Corporation). Protein identifications were obtained by searching databases of *Mus musculus* (release 2011_12, Uniprot) using tryptic cleavage, 1 missed cleavage allowed, fixed carbamidomethyl-cysteine modification and variable methionine oxidation. All data are deposited in PRIDE: PXD001633.

2.8. ABP labeling of GCase

Homogenate of tissue (50 μg total protein) was incubated with 100 nM of red BODIPY-containing MDW941 [41] in 150 mM McIlvaine buffer (150 mM citrate-Na_2HPO_4, pH 5.2 with 0.2 % (*w*/*v*) sodium taurocholate, 0.1 % Triton X-100) and protease inhibitor cocktail (Roche) for 45 min at 37 °C. Subsequently protein was denatured in 5× Laemmli buffer (50 % (*v*/v) 1 M Tris-HCl, pH 6.8, 50 % (v/v) glycerol, 10 % (w/v) DTT, 10 % (w/v) SDS, 0.01 % (w/v) bromophenol blue) by boiling for 10 min at 100 °C and separated by electrophoresis on 10 % (w/v) acrylamide SDS-PAGE gels running at 90 V. Wet slab gels were scanned for red fluorescence using a Typhoon variable mode imager (Amersham Bioscience) using λ_{ex} 532 nm and λ_{em} 610 nm (band pass filter 30 nm). ABP emitted fluorescence was quantified using ImageJ software (NIH, USA). Gels were electroblotted onto a nitrocellulose membrane (Schleicher & Schuell) and the proteins bands detected with Ponceau S staining.

2.9. Enzymatic assays

Activity measurements, in technical duplicates, were performed for GCase as described [48]. Activity was measured with 3.73 mM 4-methylumbelliferyl-β-d-glucopyranoside (4-MU-β-d-Glc), dissolved in 150 mM McIlvaine buffer (pH 5.2 supplemented with 0.2 % (*w*/*v*) sodium taurocholate, 0.1 % (*v*/v) Triton X-100) and 0.1 % BSA. The reaction was stopped with NaOH-glycine (pH 10.3), and fluorescence was measured with a fluorimeter LS55 (Perkin-Elmer, Beaconsfield, UK) at λ_{ex} 366 nm and λ_{ex} 445 nm. A total of 8 animals (4 *wt*; 4 *Limp2* −/−), at the age of 4 months of age, uniformly divided by sex, were analyzed.

2.10. HPLC and LC-MS/MS lipid measurements

Neutral glycosphingolipids, globotriaosylsphingosine (LysoGb3), GlcSph and GlcChol were determined in technical duplicates, in the homogenates as described earlier [45,49,50]. An internal standard mix ($^{13}C_5$-LysoGb3, $^{13}C_5$-GlcSph and $^{13}C_6$-GlcChol) was added to the samples for calculation. After protein precipitation with $CHCl_3$:MeOH 1:1 (v:v), one step of extraction and two washing steps were carried out, always

with the ratio $CHCl_3$:MeOH:aq (volume sample + 100 mM ammonium formate buffer pH 3.15) 1:1:0.9 (v:v:v). With this procedure, LysoGb3 and GlcSph are in the hydrophilic phase (upper phase), and GlcChol and neutral lipids will be in the hydrophobic phase (lower phase). The upper phase was dried under N_2 gas stream and the residue redissolved in MeOH (LysoGb3 and GlcSph). One-half of the lower phase, for GlcChol measurement, was dried under a N_2 gas stream and the residue redissolved in 10 mM ammonium formate in MeOH. Lipids were measured using an Acquity TQD (Waters Inc.). For determination of neutral glycosphingolipids, ceramide (Cer), GlcCer, lactosylceramide (LacCer), and globotriosylceramide (Gb3), a known amount of internal standard (C_{17}-Sphinganine) was added to the sample after the extraction, next dried under N_2 gas stream and then deacylated with 0.1 M NaOH in MeOH in a microwave for 1 h. Neutral lipids were next analyzed using a Dionex HPLC system with a C18 reversed-phase chromatography and on-line derivatisation with fluorescent o-phthaldialdehyde (OPA). The fluorescent derivatized structures derived from glycosphingolipids were quantitatively detected by measurement of fluorescence at λ_{ex} 340 nm and λ_{ex} 435 nm. Quantification of GlcCer in brain and sciatic nerves required an optimized protocol given the abundant presence of interfering galactosylceramide (GalCer) in these materials. After total lipid extraction by modified Folch extraction [51], neutral glycosphingolipids were separated from neutral lipids (ceramides and phospholipids) by solid phase extraction (SPE) using a silica gel (SiOH) SPE column [52]. After deacylation with sphingolipid ceramide N-deacylase (SCDase, Takara Bio Inc., Japan), GlcCer was digested with recombinant GCase (Imiglucerase, Genzyme) [53].

2.11. Cholesterol measurement

Cholesterol levels in the tritosome samples were assessed as described previously for cellular lysates [54] and normalized to the protein content as determined by BCA protein kit (see above).

2.12. RNA extraction and quantitative RT-PCR

Total RNA was harvested from cells using the Total RNA mini kit (Bio-Rad) or Trizol reagent (Invitrogen) according to the manufacturer's instructions. cDNA was made using the iScript cDNA synthesis kit (Bio-Rad). Real-time reverse transcription PCR was performed using the MyIQ system (Bio-Rad) and the primer LIMP-2 forward (*5′*-TTGGCCCTCTGGACATTATC-*3′*) and the LIMP-2 reverse (*5′*-AGAACCG-CATGAAGTGAACC-*3′*). Acidic ribosomal phosphoprotein P0 was determined as an internal control for cDNA content of the samples with the primer P0 forward (*5′*-TCGACAATGGCAGCATCTAC-*3′*) and P0 reverse (*5′*-ATCCGTCTCCACAGACAAGG-*3′*).

2.13. SDS-PAGE Western-blotting

Homogenates containing 20 μg of total protein were denatured in 5× Laemmli buffer (50 % (*v*/v) 1 M Tris-HCl, pH 6.8, 50 % (v/v) glycerol, 10 % (*w*/*v*) DTT, 10 % (w/v) SDS, 0.01 % (w/v) bromophenol blue) by boiling for 10 min at 100 °C, and separated by electrophoresis on 10 % acrylamide (w/v) SDS-PAGE gels running at 90 V. SDS–PAGE gels were electroblotted onto a nitrocellulose membrane (Schleicher & Schuell). Membranes were blocked with 5 % skimmed milk and 0.05 % Tween-20 in Tris-buffered saline (TBS) for 1 h at room temperature and incubated overnight with the rabbit polyclonal anti-LIMP-2 antibody (NB400-129, Novus Biologicals) at 4 °C. Membranes were then washed three times with 0.01 % Tween-20 in TBS and incubated with the appropriate IRDye conjugated secondary antibody for 1 h at room temperature. After washing, detection was performed using the Odyssey® Clx. Infrared Imaging System (LI-COR).

3. Results

3.1. Active GCase in tissues of Limp2 −/− mice as determined by enzymatic activity measurement

Various tissues were collected from *Limp2* −/− and *wt* mice of 4 months of age. In tissue homogenates, GCase activity was measured with the fluorogenic substrate 4-MU-β-d-Glc (Table 1). Activity was very low in many of the tissues analyzed (eye, pancreas, heart, spleen, liver and lungs) when compared to *wt* materials. In the case of the intestine (divided in duodenum, ileum and jejunum), no clear differences were observed in the enzymatic activity between the genotypes, probably due to the abundance of bacterial glycosidases as well as endogenous lactase-phloridzin hydrolase (LPH), which also hydrolyzes the artificial substrate [42]. Of interest, in the case of leukocytes (peripheral blood mononuclear cells - PBMC), brain, and skin, a significant but less prominent reduction of GCase activity was found in *Limp2* −/− mice when compared to other organs (Table 1). Of note, plasma from *wt* animals contains virtually no GCase activity, but the activity is detectable in plasma of *Limp2* −/− mice, likely due to faulty secretion of the mistargeted enzyme. No striking abnormalities were noted in levels of other lysosomal enzymes (e.g., β-glucuronidase, β-hexosaminidase, α-galactosidase) examined in tissues of LIMP-2 deficient mice as compared to *wt* animals (data not shown).

3.2. Detection of active GCase molecules in tissues by ABP labeling

The same tissue homogenates were incubated with ABP MDW941 to detect active GCase following SDS-PAGE and fluorescence scanning (Fig. 1). In general, tissues of *Limp2* −/− mice showed absence or a strongly reduced amount of active GCase, when compared to controls. We ranked tissues of *Limp2* −/− mice based on their residual enzyme activity measured in vitro (Fig. 2A). Compared to Fig. 2B is the residual GCase activity determined by enzymatic assay and ABP labeling. A very strong correlation between the results obtained with both methods is

Table 1
GCase activity in several tissues obtained from *Limp2* −/− mice and matched *wt* animals at 4 months of age. Expressed as nmol/h/g wet weight; for plasma in nmol/h/mL; for leukocytes nmol/h/mg protein. $N = 4$ per genotype.

Tissue	GCase activity	
	Wt (mean ± SD)	*Limp2* −/− (mean ± SD)
Duodenum	728.58 ± 262.33	463.51 ± 54.80
Jejunum	660.35 ± 167.74	812.48 ± 23.79
Liver	142.05 ± 31.02	22.65 ± 11.43
Ileum	114.95 ± 20.20	78.20 ± 51.22
Testis (TE)	103.23 ± 10.02	39.85 ± 3.32
Thymus	98.06 ± 35.16	27.23 ± 9.45
Abdominal fat (AF)	96.79 ± 33.68	16.44 ± 3.79
Bone Marrow (BM)	96.34 ± 7.65	21.09 ± 1.06
Pancreas	94.77 ± 20.09	9.81 ± 2.20
Omental fat (OF)	93.13 ± 22.63	16.16 ± 2.47
Epidydimal fat (EF)	90.02 ± 35.69	16.96 ± 3.96
Epididymis (EP)	88.01 ± 26.59	45.33 ± 32.51
Inguinal fat (IF)	79.57 ± 24.69	10.81 ± 6.32
Lymph node (LN)	62.88 ± 2.21	20.59 ± 1.93
Spleen	60.30 ± 13.20	10.79 ± 2.52
Adrenal gland (AG)	58.00 ± 3.82	18.64 ± 0.35
Lungs	57.36 ± 12.87	9.59 ± 0.83
Salivary gland (SG)	55.97 ± 10.60	16.27 ± 1.52
Brain	54.20 ± 0.69	32.14 ± 2.74
Brown adipose tissue (BAT)	48.92 ± 1.35	11.41 ± 4.02
Leukocytes	46.78 ± 2.98	31.73 ± 1.47
Kidney	34.94 ± 4.11	9.76 ± 0.51
Skin	33.39 ± 4.24	18.75 ± 2.03
Heart	29.32 ± 6.03	3.95 ± 1.29
Sciatic nerve (SN)	23.97 ± 0.46	22.36 ± 12.78
Eye	4.65 ± 2.05	0.85 ± 0.28
Plasma	0.78 ± 0.10	8.48 ± 1.59

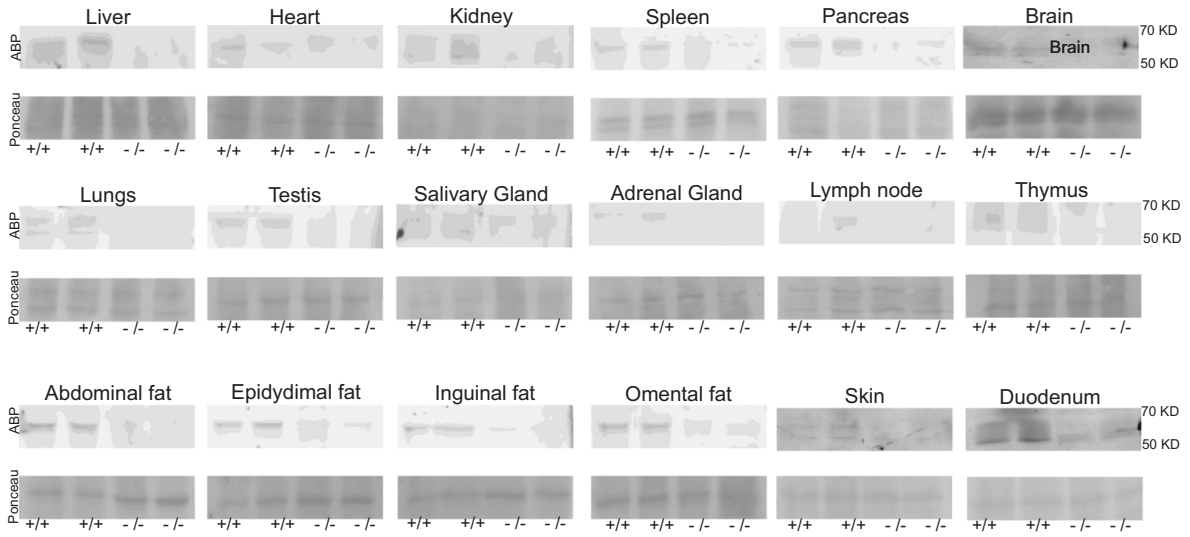

Fig. 1. Visualization of GCase with fluorescent ABP MDW941. Upper panel: Detection of active GCase in tissues and organs homogenates (50 μg) labelled with ABP followed by SDS-PAGE and visualization by fluorescence imaging. (+/+) = *wt*; (−/−) = *Limp2* −/− mice. Lower panel: Ponceau total protein staining.

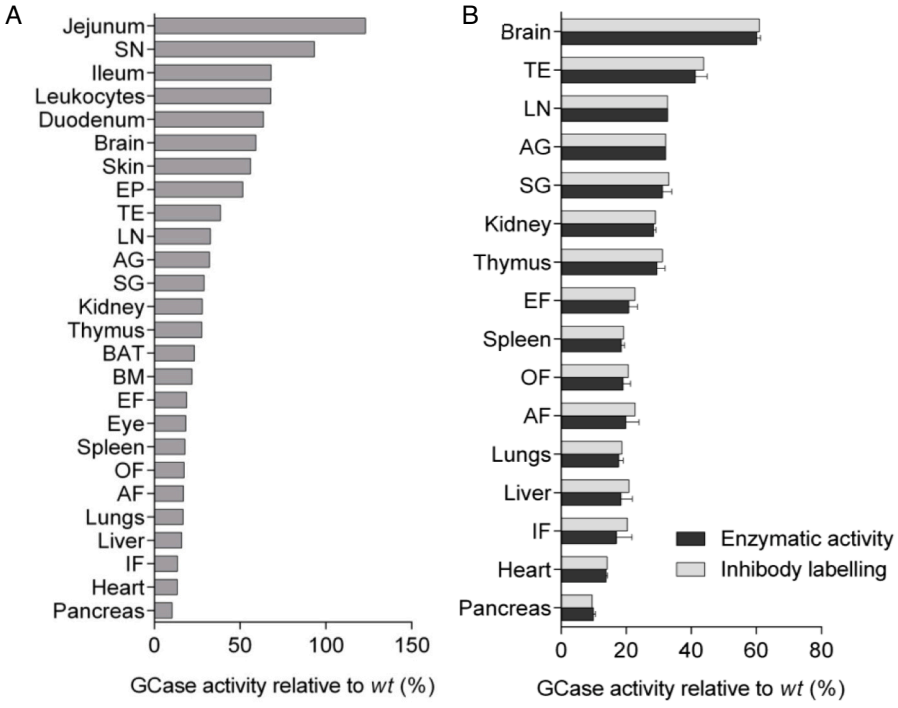

Fig. 2. Residual GCase activity in tissue of *Limp2* −/− mice at 4 months of age. A. Ranking of the homogenates according to the residual enzymatic activity. B. Comparison of residual GCase activity by enzymatic assay and ABP labeling.

apparent. Fig. 2 illustrates the marked tissue dependence of GCase reduction during LIMP-2 deficiency. Of note, considerable residual GCase, albeit significantly reduced, was detected for brain, leukocytes and sciatic nerve (SN) when determined by enzymatic assay or ABP labeling.

3.3. Detection of lipid metabolite abnormalities in *Limp2* −/− mice

To assess the functional deficiency of GCase, we analyzed lipid metabolites in various tissues of *Limp2* −/− mice. Given the fact that GlcCer is the primary storage lipid during GCase deficiency, we first determined its concentration in various tissues of *Limp2* −/− and *wt* animals. Of note, the presented values for hexosylceramide (HexCer) in brain and SN are the sum of GalCer and GlcCer, which were indistinguishable with the procedure used. Hence, the use of the terms HexCer and HexSph. It is known that in most mouse tissues the majority of HexCer reflects GlcCer, as confirmed by its digestion by recombinant GCase [53]. An exception is the brain that has a relatively high GalCer content and to a lesser extent the kidney. In our experience, hexosylsphingosine (HexSph) in peripheral tissues is almost exclusively glucosylsphingosine (GlcSph). Table 2 shows that HexCer concentrations vary among tissues and that HexCer is most prominently elevated in leukocytes, omental fat (OF), abdominal fat (AF) and lymph node (LN) of *Limp2* −/− mice.

Next, we measured the concentrations of HexSph. As in GD, much clearer abnormalities were detected for HexSph, being elevated in almost every tissue, most strikingly in pancreas, heart and OF (Table 2).

Table 2
HexCer (GlcCer) and HexSph (GlcSph) levels in tissues of *Limp2* −/− and *wt* mice at 4 months of age. For GlcCer, tissue levels are expressed in nmol/g wet weight tissue; leukocytes in nmol/mg protein; plasma, bile and urine in nmol/mL. In the case of GlcSph, tissue levels are expressed in pmol/g wet weight tissue; leukocytes in pmol/mg protein; plasma, bile and urine in pmol/mL. *Hexosylceramide = GalCer + GlcCer; $^{+}$Hexosylsphingosine = GalSph + GlcSph. $N = 6$ per genotype.

Tissue/ organ	HexCer*			HexSph^{+}		
Genotype	*Wt* (mean ± SD)	*Limp2* −/− (mean ± SD)	*Limp2* −/−: *wt ratio*	*Wt* (mean ± SD)	*Limp2* −/− (mean ± SD)	*Limp2* −/−:*wt ratio*
Pancreas	9.6 ± 4.3	15.4 ± 1.9	1.61	2.3 ± 0.7	178.4 ± 24.1	76.55
Heart	4.2 ± 2.6	3.0 ± 0.4	0.72	3.3 ± 1.0	86.7 ± 20.5	26.04
Inguinal fat	8.2 ± 6.3	27.5 ± 11.9	3.37	3.0 ± 0.9	31.9 ± 17.5	10.64
Liver	22.2 ± 13.3	23.4 ± 13.0	1.06	32.1 ± 2.6	214.9 ± 157.9	6.70
Lungs	30.5 ± 9.5	42.5 ± 14.8	1.39	34.9 ± 8.0	738.4 ± 285.0	21.18
Abdominal fat	8.8 ± 5.1	57.7 ± 29.3	6.59	1.9 ± 0.7	40.5 ± 35.7	20.88
Omental fat	3.3 ± 1.5	14.7 ± 4.4	4.35	1.0 ± 0.7	128.4 ± 41.0	132.41
Spleen	75.0 ± 8.0	73.8 ± 6.6	0.98	20.6 ± 2.3	400.0 ± 143.7	19.37
Eye	571.8 ± 179.1	171.0 ± 107.2	0.30	62.9 ± 5.7	892.6 ± 189.7	14.19
Epididymal fat	3.5 ± 2.0	3.9 ± 0.4	1.13	4.2 ± 1.9	11.0 ± 0.2	2.61
Bone Marrow	0.5 ± 0.3	0.7 ± 0.4	1.49	0.2 ± 0.1	2.0 ± 0.8	10.05
Brown adipose tissue	32.6 ± 15.2	41.2 ± 10.2	1.26	4.1 ± 1.7	49.7 ± 38.8	12.20
Thymus	70.54 ± 13.6	70.9 ± 15.4	1.01	13.4 ± 2.4	85.6 ± 23.1	6.37
Kidney	17.8 ± 4.5	7.8 ± 10.2	0.44	25.8 ± 0.7	557.5 ± 115.4	21.59
Salivary gland	22.6 ± 8.6	41.4 ± 9.6	1.83	5.0 ± 1.6	95.2 ± 37.4	19.15
Adrenal gland	33.2 ± 12.4	53.4 ± 26.2	1.61	7.0 ± 5.1	75.7 ± 65.1	10.75
Lymph node	40.0 ± 20.2	97.5 ± 28.5	2.44	5.0 ± 4.3	95.6 ± 69.0	19.23
Testis	13.4 ± 2.5	13.3 ± 6.0	0.99	5.2 ± 1.8	24.7 ± 7.0	4.77
Epididymal	13.3 ± 6.7	14.0 ± 5.9	1.05	29.4 ± 4.3	233.2 ± 112.1	7.93
Skin	23.3 ± 5.1	23.7 ± 14.2	1.02	9.3 ± 4.9	29.6 ± 13.6	3.20
Brain*	3067 ± 837	3249 ± 474	1.06	112.8 ± 5.8	230.5 ± 14.5	2.04
Duodenum	64.3 ± 7.1	68.4 ± 9.0	1.06	8.8 ± 3.8	139.0 ± 26.5	15.81
Leukocytes	0.1 ± 0.1	0.7 ± 0.8	7.30	0.3 ± 0.3	1.7 ± 0.3	5.57
Ileum	25.1 ± 3.8	28.1 ± 5.5	1.12	9.3 ± 1.3	180.5 ± 22.9	19.39
Sciatic nerve*	10,493 ± 1020	4898 ± 1016	0.47	1112 ± 652	861 ± 544	0.77
Jejunum	41.4 ± 9.2	47.9 ± 11.2	1.16	8.2 ± 1.6	140.7 ± 15.3	17.24
Plasma	3.2 ± 0.9	1.8 ± 1.1	0.57	1.1 ± 1.3	3.6 ± 1.7	3.13
Bile	4.8 ± 5.7	2.1 ± 0.8	0.43	1.4 ± 0.5	6.3 ± 2.2	4.54
Urine	0.3 ± 0.1	0.2 ± 0.1	0.73	0.6 ± 1.2	0.4 ± 0.2	0.55

A trend is apparent between HexSph accumulation and residual GCase activity in tissues. Exceptions in this regard are the OF, kidney, salivary gland (SG), LN and the different parts of the intestine.

The concentrations of GlcChol in tissues of *Limp2* −/− and *wt* mice were also determined (supplemental Table S1). Marked elevations of GlcChol were detected in the plasma, liver, pancreas and fat of *Limp2* −/− mice compared to *wt*.

3.4. Analysis of lysosomes (tritosomes) from liver of *Limp2* −/− and *wt* mice

3.4.1. Proteome of tritosomes

To investigate whether lack of LIMP-2 also impairs other lysosomal matrix proteins besides GCase, we analyzed the protein composition of isolated lysosomes (tritosomes) from *wt* and *Limp2* −/− mice using LC-MS/MS. Importantly, both GCase and LIMP-2 protein were found to be absent in tritosomes from *Limp2* −/− mice. Around 70 lysosomal matrix proteins were identified and quantified. Table 3A shows the major reduction in GCase in LIMP-2 deficient tritosomes and it reveals that lysosomal acid lipase, sphingomyelin phosphodiesterase, cathepsin C and β-galactosidase 1 are about two-fold decreased compared to *wt*. About two-fold increases were noted for cathepsin H and *N*-acetylglucosamine 6 sulfatase. The proteomics analysis (see also supplemental Table S2) indicates that LIMP-2 deficiency results in a very specific deficiency in GCase and seems not to affect other lysosomal proteins, at least in the studied liver cell populations.

3.4.2. Glycolipid content of tritosomes

We next determined the glycolipid content of tritosomes isolated from liver of *wt* and *Limp2* −/− mice. No major differences were noted in concentrations of any of the neutral glycosphingolipids Cer, GlcCer, LacCer, and Gb3, and the sphingoid bases, lysoGb3. Only a prominent increase in HexSph (3.1 vs 30.1 pmol/mg protein) and GlcChol (17.5 vs 66.0 pmol/mg protein) was detected. Total cholesterol (142 vs 159 nmol/mg protein) and especially cholesterol-ester (18 vs 33 nmol/mg protein) tended to be elevated in LIMP-2 deficient tritosomes (Table 3B).

3.5. Clinical course of disease in LIMP-2 deficient mice

Disease manifestation is relatively benign in *Limp2* −/− mice. As

Table 3
Proteins and lipids in tritosomes.

A. Examples of differential proteins in tritosomes isolated from *Limp2* −/− and *wt* mice. For an extended list see supplemental Table S1.

Accession no.	Protein	*Limp2* −/−: wt ratio
P17439	Glucosylceramidase	Not detectable in *Limp2*−/−
Q9Z0M5	Lysosomal acid lipase	0.44
Q04519	Sphingomyelin phosphodiesterase	0.59
E9Q2Q0	Cathepsin C	0.59
F7AF87	Acid beta-galactosidase1	0.60
D3Z437	Cathepsin H	2.14
Q571E4	N acetylgalactosamine 6 sulfatase	2.16

B. Selected lipids in tritosomes isolated from *Limp2* −/− and *wt* mice.

Lipid	Tritosomes *wt*	Tritosomes *Limp2* −/−	*Limp2* −/−: wt ratio
HexSph (pmol/mg of protein)	3.1	30.1	10
GlcChol (pmol/mg of protein)	17.5	66	3.8
Total cholesterol (nmol/mg of protein)	142	159	1.1
Cholesterol-ester (nmol/mg of protein)	18	33	1.8

shown in supplemental Fig. S1, despite the clear absence of lysosomal GCase in hepatocytes, no abnormalities in the liver were noted. Actually, no overt pathology was detected by an experienced pathologist in any organs of mice of 6 and 12 months of age except for signs of hydronephrosis (upper urinary tract dilation) in the absence of clear abnormalities in the glomerulus and signs of brain pathology [29]. Of interest, a marked thickness of sciatic nerve (SN) was observed (supplemental Fig. S2).

3.6. Biochemical course of disease

Given the detected abnormalities in lipid metabolites in tissues of *Limp2* −/− mice of 4 months of age, we next studied how these abnormalities develop with age in several tissues. HexCer changes were very small in all tissues from *Limp2* −/− mice when examined at various ages (Fig. 3). Only a very slight increase was noted for the kidney and SG at an older age. In the case of the eye of *Limp2* −/− mice, a significant reduction of HexCer was observed. In sharp contrast, HexSph elevation was already detectable in animals of 2 months of age and generally did not further increase with age (Fig. 4), except for the thymus of *Limp2* −/− mice. GlcChol in tissues was already increased at the youngest age examined (2 months). In none of the tissues a marked accumulation of GlcChol with increasing age was observed (supplemental Fig. S3). The concentrations of globosides Gb3 and lysoGb3 were also determined. No differences from *wt* animals at different ages were detected, except for reduced levels in spleen (data not shown).

3.7. Glycolipids in brain and SN

In most tissues GlcCer concentrations are known to be far higher than those of its isomer GalCer, but in brain and nerves, GalCer is abundant. Our HPLC procedure does not fully separate GlcCer and galactosylceramide. In the case of the brain of *Limp2* −/− mice, we observed no differences in the levels of HexCer and HexSph (see Figs. 3 and 4, respectively). In the case of SN, HexCer was significantly reduced and less prominently HexSph. Treatment of brain and SN homogenates with excess recombinant GCase allows the discrimination between Glc- and GalCer since the recombinant enzyme only degrades GlcCer. Almost no differences in the total HexCer (GlcCer + GalCer) *wt* and *Limp2* −/− mice brain were observed, at any age examined (Fig. 3). Treatment with recombinant GCase revealed that the GlcCer content of brain from *Limp2* −/− mice is normal (Fig. 5). Only a small decrease in GalCer is demonstrable. In the SN, clear abnormalities in HexCer are detected, in particular a reduction in GalCer is apparent with increasing age which might point to demyelination. Already at young age, the concentration of ceramide is elevated in the SN, reaching a maximum at 4 months, and being reduced after that.

4. Discussion

The availability of a mouse model of AMRF, *Limp2* −/− mice, allowed us to carefully investigate abnormalities in GCase during genetic loss of LIMP-2. Enzymatic activity measurements demonstrated great variation among tissues in deficiency of GCase. An independent method to specifically assess the presence of active GCase molecules using a fluorescent ABP, revealed consistent differences among tissues regarding the decrease of active GCase. Tissues like pancreas, heart and liver show major reductions in GCase in mice lacking LIMP-2. In contrast, leukocytes of the same animals show a relatively high residual GCase reaching about 65 % of normal values. The same has been observed for AMRF patients. Residual GCase is relatively high in leukocytes and lymphoblasts of these patients [30,56]. The high residual GCase capacity of leukocytes prevents formation of GlcCer-laden macrophages in AMRF patients as is characteristic for GD patients. GlcCer laden Gaucher cells accumulate in spleen, liver and bone marrow of GD patients accompanied by marked hepatosplenomegaly [1]. Such visceral symptoms do not occur in AMRF patients. The high residual GCase in white blood cells of AMRF patients, and *Limp2* −/− mice, likely contributes to the remarkably discordant manifestation of GD and AMRF. We looked for a mechanism explaining the remarkable high residual GCase content of leukocytes. It was hypothesized that phagocytic white blood cells might be relatively successful in capturing faulty secreted GCase during LIMP-2 deficiency and deliver it to their lysosomes. As described in the supplemental addendum, THP1 cells and lymphoblasts with reduced LIMP-2 were found to show uptake of extracellular GCase through (dynamin-dependent) endocytosis, a process contributing significantly to intracellular enzyme activity. Such corrective uptake of GCase takes place far less efficiently by LIMP-2 deficient fibroblasts. The experiments conducted with cultured cells rendered data consistent with the hypothesis formulated above. However, it should be kept in mind that cell culture experiments do not render conclusive evidence for corrective mechanisms occurring in GCase content of white blood cells of LIMP-2 deficient mice and AMRF patients.

Our study revealed glycolipid abnormalities developing during LIMP-2 deficiency. Firstly, the primary substrate of GCase GlcCer (measured as HexCer), was found to be increased in tissues of *Limp2* −/− mice, but only slightly in view of the marked GCase deficiencies. On the other hand, GlcSph measured as HexSph, formed by lysosomal deacylation of accumulating GlcCer [44], is strongly increased in LIMP-2 deficient tissues. In general, GlcSph is highest in tissues of *Limp2* −/− mice with the lowest GCase. The maximal increase in tissue GlcCer and GlcSph occurs already at two months of age. The observed equilibrium in GlcCer might be due to down-regulation of synthesis or activation of its removal from cells by exocytic pathways. GlcSph might be less formed upon reduced GlcCer supply to lysosomes or actively reduced by the cytosolic enzyme GBA2 or its secretion from the body via liver and bile [44]. An exception in this respect are leukocytes from *Limp2* −/− mice. Because of their high residual GCase, these cells hardly accumulate GlcCer and form GlcSph. In summary, our findings with *Limp2* −/− mice differ quite clearly from those of GD mouse models with inducible GCase deficiency in cells of the white blood cell lineage: these animals show accumulation of GlcCer-laden macrophages in tissues with age [56,57]. GlcChol, the most recently identified glycolipid, was found to be clearly elevated in tissues of *Limp2* −/− mice, reminiscent of findings in GD patients and in mouse models with reduced GCase activity [45]. Whether the noted increases in GlcChol have pathophysiological consequences is presently still unknown. It has been hypothesized that excessive GlcChol may have detrimental effects on lipid raft composition and function [56].

Mice lacking LIMP-2 develop, at old age, tubular proteinuria, as reported for some AMRF patients [4,19,40]. At the age of 4 months, no overt proteinuria occurs yet in the *Limp2* −/− mice and their kidney shows similar residual GCase levels to other tissues. Likewise, lipid abnormalities are comparable to those in other tissues. Spleen and liver show no hypertrophy, as occurs in GD, and are similar in GCase and lipid abnormalities to other tissues. Brain of *Limp2* −/− mice shows a slightly higher residual GCase compared to viscera but no remarkable difference in lipid abnormalities. Possibly, we missed in our brain analyses specific lipids abnormalities in neuronal cells associated with epileptic attacks as occur in AMRF patients. Abnormal GlcCer metabolism seems to be strongly associated with neuropathology. Severe cases of GD develop characteristic neuropathology and even type I GD patients as well as carriers of mutated *GBA1* have an increased risk for developing Parkinsonism and Lewy-Body dementia [59]. Michelakakis and colleagues were the first to report a similar increased risk imposed by heterozygosity for *SCARB2* mutations, a finding independently confirmed by others [60–62]. *Limp2* −/− mice have been also found to develop α-synuclein deposits and associated pathology of dopaminergic neurons [29]. Recent studies have identified 15 genetic enhancers of α-synuclein-induced locomotor dysfunction related to lysosomal storage disorder (LSD) genes, reinforcing their role in Parkinson's disease (PD) pathogenesis [63,64]. These include homologs of *GBA*, *SCARB2* and

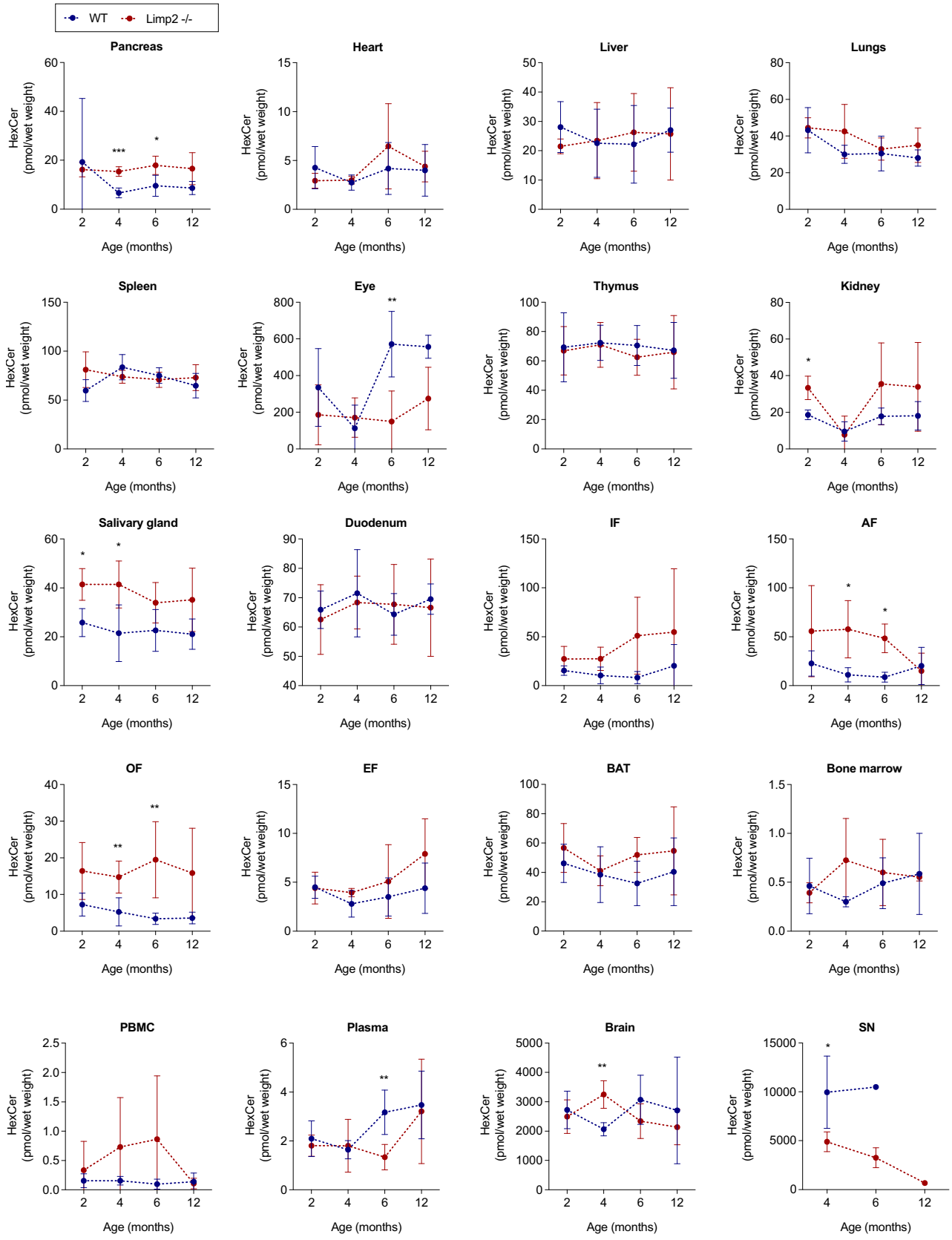

Fig. 3. HexCer levels in wt and *Limp2* −/− mice at different ages.

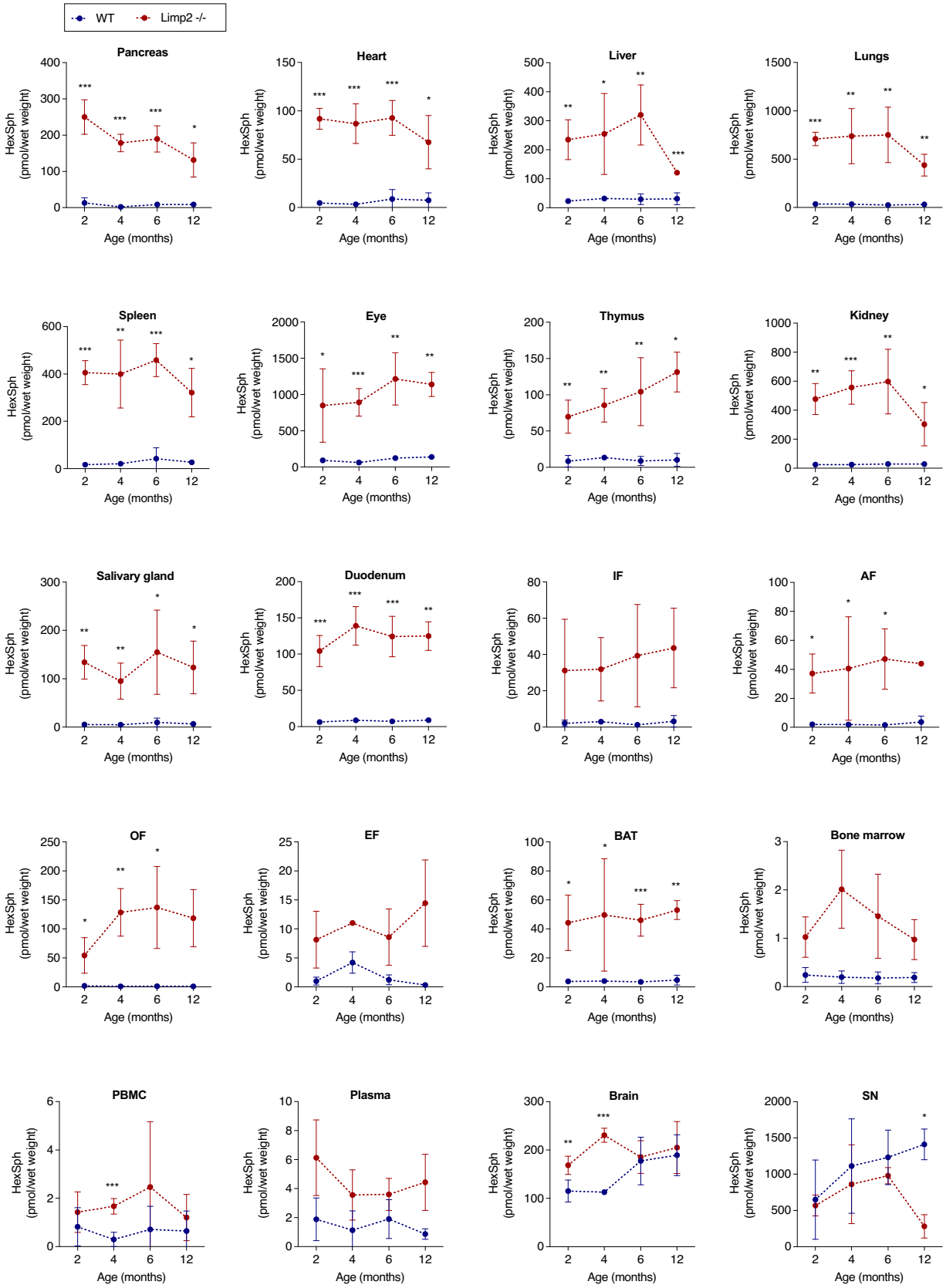

Fig. 4. HexSph levels in wt and *Limp2* −/− mice at different ages. Data are presented as mean ± SD of N = 6 per genotype and age. *P* values were obtained by unpaired *t*-test; ***$P < 0.001$; **$P < 0.01$; *$P < 0.05$.

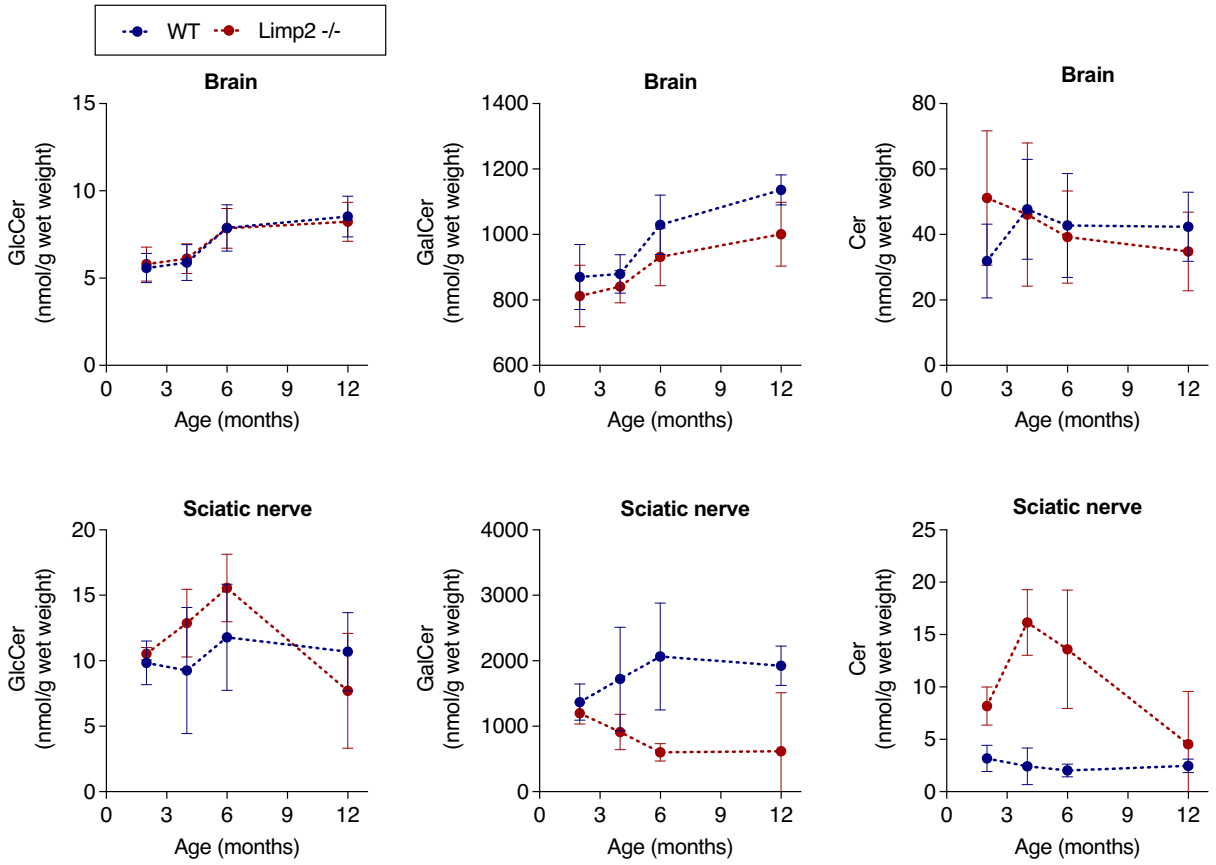

Fig. 5. Glycosphingolipids and ceramide levels in brain and sciatic nerve. Lipids were determined as described in M&M. To distinguish GlcCer and GalCer digestion with GCase was performed. GalCer is no substrate for the enzyme. Data are presented as mean ± SD N = 6 per genotype and age. *P* values were obtained by unpaired *t*-test; ***$P < 0.001$; **$P < 0.01$; *$P < 0.05$.

other LSD genes with independent support as PD susceptibility factors. The research implicates several metabolic pathways, particularly cholesterol homeostasis, in α-synuclein-mediated neurotoxicity. Disturbed cellular cholesterol metabolism, in GBA1-associated PD models, could contribute to changes in lipid rafts and synaptic integrity [65]. Alterations in brain cholesterol metabolism and neurotransmission occur in early stages of neurodegenerative diseases, with polymorphisms in genes associated with cholesterol homeostasis affecting disease risk and severity [66]. These findings highlight the importance of cholesterol balance in synaptic function and its potential role in PD and other neurodegenerative disorders.

A hallmark of LIMP-2 deficiency in man is peripheral demyelinating neuropathy [30]. We observed grossly swollen SN in *Limp2* −/− mice at relatively young age. In the SN of *Limp2* −/− mice, residual GCase is relatively high, and GlcCer and HexSph levels are close to normal. The markedly elevated ceramide might be more closely linked to the pathology. The noted reduction in GalCer in SN of *Limp2* −/− mice is likely to reflect ongoing peripheral demyelination reflected by the tremors observed in animals.

The analysis of highly purified lysosomes from hepatocytes of *Limp2* −/− and *wt* mice revealed that except for the absence of GCase most other lysosomal matrix proteins appear normal in LIMP-2 deficiency. Of interest are the about two-fold reduced levels of acid lipase and acid sphingomyelinase, two enzymes involved in lysosomal lipid catabolism. The tritosomes from hepatocytes of *Limp2* −/− mice showed significant increases in HexSph (nearly ten-fold) and GlcChol (nearly four-fold). These abnormalities resemble findings made during primary GCase deficiency. A clear increase in cholesterol-ester and to a lesser extent cholesterol was observed. This might be partly due to the reduced acid lipase that normally converts cholesterol-ester to cholesterol in lysosomes. Moreover, compelling evidence has been presented for a direct role of LIMP-2 in cholesterol export from lysosomes [33]. Noteworthy, the prominent absence of GCase in lysosomes seems not to markedly affect hepatocytes macroscopically or in their function. This finding points to very effective, but still not identified, compensatory mechanisms in these cells avoiding lysosomal storage of GlcCer.

In conclusion, our study sheds new light on the consequences of systemic LIMP-2 deficiency regarding tissue specific GCase reductions and associated compensatory deacylation of GlcCer to GlcSph. Although most tissues lacking LIMP-2 present a marked deficiency in GCase, leukocytes appear relatively protected, possibly by phagocytic re-uptake of secreted GCase by other cells. This offers a plausible explanation for the remarkable prominent difference in symptomatology of AMRF and GD.

CRediT authorship contribution statement

Paulo Gaspar: Writing – review & editing, Writing – original draft, Validation, Methodology, Investigation, Formal analysis, Conceptualization. **André R.A. Marques:** Writing – review & editing, Writing – original draft, Validation, Investigation, Formal analysis, Conceptualization. **Maria J. Ferraz:** Writing – review & editing, Writing – original draft, Methodology, Investigation, Formal analysis, Conceptualization. **Markus Damme:** Writing – original draft, Methodology, Investigation, Formal analysis. **Gertjan Kramer:** Validation, Methodology, Investigation, Formal analysis. **Mina Mirzaian:** Writing – original draft, Methodology, Investigation, Formal analysis. **Marion Gijbels:** Visualization, Validation, Methodology, Investigation. **Roelof Ottenhoff:** Validation, Methodology, Investigation, Formal analysis, Data curation, Conceptualization. **Cindy van Roomen:** Visualization, Formal analysis, Data

curation, Conceptualization. **Herman S. Overkleeft:** Visualization, Validation, Methodology, Formal analysis. **Michael Schwake:** Writing – original draft, Validation, Formal analysis, Conceptualization. **Saskia Heybrock:** Validation, Methodology, Investigation. **Maria Carmo Macário:** Resources, Data curation. **Paul Saftig:** Writing – review & editing, Writing – original draft, Supervision, Resources, Project administration, Methodology, Funding acquisition, Formal analysis, Data curation, Conceptualization. **Johannes M. Aerts:** Writing – review & editing, Writing – original draft, Supervision, Resources, Project administration, Methodology, Investigation, Funding acquisition, Data curation, Conceptualization.

Declaration of competing interest

The authors declare the following financial interests/personal relationships which may be considered as potential competing interests: Andre Marques reports financial support was provided by Foundation for Science and Technology. Paulo Gaspar reports financial support was provided by Foundation for Science and Technology. If there are other authors, they declare that they have no known competing financial interests or personal relationships that could have appeared to influence the work reported in this paper.

Acknowledgements

This work was funded by Fundação para a Ciência e Tecnologia (SFRH/BD/72862/2010 to P.G) and PTDC/SAU-GMG/105344/2008. ARAM was funded by the FCT Stimulus of Scientific Employment Individual Support Call 2017 (CEECIND/01006/2017).

The authors extend the deepest gratitude to Dr. Clara Sá Miranda for her invaluable initiative, guidance and support in every stage of this research project.

Appendix A. Supplementary data

Supplementary data to this article can be found online at https://doi.org/10.1016/j.bbalip.2025.159657.

Data availability

Data will be made available on request.

References

[1] E. Beutler, G.A. Grabowski, Glucosylceramide lipidosis-Gaucher disease, in: C. R. Scriver, A.L. Beaudet, W.S. Sly, D. Valle (Eds.), The Metabolic and Molecular Bases of Inherited Diseases, 8th Ed, McGraw-Hill, New York, 2001.

[2] D. Reczek, M. Schwake, J. Schröder, H. Hughes, J. Blanz, X. Jin, W. Brondyk, S. Van Patten, T. Edmunds, P. Saftig, LIMP-2 is a receptor for lysosomal mannose-6-phosphate-independent targeting of beta-glucocerebrosidase, Cell 131 (2007) 770–783.

[3] A. Balreira, P. Gaspar, D. Caiola, J. Chaves, I. Beirão, J.L. Lima, J.E. Azevedo, M.C. S. Miranda, A nonsense mutation in the LIMP-2 gene associated with progressive myoclonic epilepsy and nephrotic syndrome, Hum. Mol. Genet. 17 (2008) 2238–2243.

[4] S.F. Berkovic, L.M. Dibbens, A. Oshlack, J.D. Silver, M. Katerelos, D.F. Vears, R. Lüllmann-Rauch, J. Blanz, K.W. Zhang, J. Stankovich, R.M. Kalnins, J. P. Dowling, E. Andermann, F. Andermann, E. Faldini, R. D'Hooge, L. Vadlamudi, R. A. Macdonell, B.L. Hodgson, M.A. Bayly, J. Savige, J.C. Mulley, G.K. Smyth, D. A. Power, P. Saftig, M. Bahlo, Array-based gene discovery with three unrelated subjects shows SCARB2/LIMP-2 deficiency causes myoclonus epilepsy and glomerulosclerosis, Am. J. Hum. Genet. 82 (2008) 673–684.

[5] T. Kuronita, E.L. Eskelinen, H. Fujita, P. Saftig, M. Himeno, Y. Tanaka, A role for the lysosomal membrane protein LGP85 in the biogenesis and maintenance of endosomal and lysosomal morphology, J. Cell Sci. 115 (2002) 4117–4131, 751.

[6] R. Crombie, R. Silverstein, Lysosomal integral membrane protein II binds thrombospondin-1. Structure-function homology with the cell adhesion molecule CD36 defines a conserved recognition motif, J. Biol. Chem. 273 (1998) 4855–4863.

[7] S. Yamayoshi, K. Fujii, S. Koike, Scavenger receptor b2 as a receptor for hand, foot, and mouth disease and severe neurological diseases, Front. Microbiol. 3 (2012) 32.

[8] S. Yamayoshi, Y. Yamashita, J. Li, N. Hanagata, T. Minowa, T. Takemura, S. Koike, Scavenger receptor B2 is a cellular receptor for enterovirus 71, Nat. Med. 15 (2009) 798–801.

[9] K. Kobayashi, S. Koike, Cellular receptors for enterovirus 762 A71, J. Biomed. Sci. 27 (2) (2020).

[10] Y.-J. Fu, I. Aida, M. Tada, M. Tada, Y. Toyoshima, S. Takeda, T. Nakajima, H. Naito, M. Nishizawa, O. Onodera, A. Kakita, H. Takahashi, Progressive myoclonus epilepsy: Extraneuronal brown pigment deposition and system neurodegeneration in the brains of Japanese patients with novel SCARB2 mutations, Neuropathol. Appl. Neurobiol. 40 (2014) 551–563.

[11] L.M. Dibbens, R. Michelucci, A. Gambardella, F. Andermann, G. Rubboli, M. A. Bayly, T. Joensuu, D.F. Vears, S. Franceschetti, L. Canafoglia, R. Wallace, A. G. Bassuk, D.A. Power, C.A. Tassinari, E. Andermann, A.E. Lehesjoki, S.F. Berkovic, SCARB2 mutations in progressive myoclonus epilepsy (PME) without renal failure, Ann. Neurol. 66 (2009) 532–536.

[12] F. Hopfner, B. Schormair, F. Knauf, A. Berthele, T.R. Tölle, R. Baron, C. Maier, R.-D. Treede, A. Binder, C. Sommer, C. Maihöfner, W. Kunz, F. Zimprich, U. Heemann, A. Pfeufer, M. Näbauer, S. Kääb, B. Nowak, C. Gieger, P. Lichtner, C. Trenkwalder, K. Oexle, J. Winkelmann, Novel SCARB2 mutation in action myoclonus-renal failure syndrome and evaluation of SCARB2 mutations in isolated AMRF features, BMC Neurol. 11 (2011) 134.

[13] M. Zeigler, V. Meiner, J.P. Newman, B. Steiner-Birmanns, R. Bargal, V. Sury, G. Mengistu, O. Kakhlon, I. Leykin, Z. Argov, O. Abramsky, A. Lossos, A novel SCARB2 mutation in progressive myoclonus epilepsy indicated by reduced β-glucocerebrosidase activity, J. Neurol. Sci. 339 (2014) 210–213.

[14] J. Chaves, I. Beirão, A. Balreira, P. Gaspar, D. Caiola, M.C. Sá-Miranda, J.L. Lima, Progressive myoclonus epilepsy with nephropathy C1q due to SCARB2/LIMP-2 deficiency: clinical report of two siblings, Seizure 20 (2011) 738–740.

[15] C. Perandones, L.A. Pellene, F. Micheli, A new SCARB2 mutation in a patient with progressive myoclonus ataxia without renal failure, Mov. Disord. 29 (2014) 158–159.

[16] R. Guerrero-López, P.J. García-Ruiz, B.G. Giráldez, C. Durán-Herrera, M.R. Querol-Pascual, J.M. Ramírez-Moreno, S. Más, J.M. Serratosa, A new SCARB2 mutation in a patient with progressive myoclonus ataxia without renal failure, Mov. Disord. 27 (2012) 1826–1827.

[17] Y. Higashiyama, H. Doi, M. Wakabayashi, Y. Tsurusaki, N. Miyake, H. Saitsu, C. Ohba, R. Fukai, S. Miyatake, H. Joki, S. Koyano, Y. Suzuki, F. Tanaka, Y. Kuroiwa, N. Matsumoto, A novel SCARB2 mutation causing late-onset progressive myoclonus epilepsy, Mov. Disord. 28 (2013) 552–553.

[18] C. Perandones, F.E. Micheli, L.A. Pellene, M.A. Bayly, S.F. Berkovic, L.M. Dibbens, A case of severe hearing loss in action myoclonus renal failure syndrome resulting from mutation in SCARB2, Mov. Disord. 27 (2012) 1200–1201.

[19] M.J. Desmond, D. Lee, S.A. Fraser, M. Katerelos, K. Gleich, P. Martinello, Y.Q. Li, M.C. Thomas, R. Michelucci, A.J. Cole, P. Saftig, M. Schwake, D. Stapleton, S. F. Berkovic, D.A. Power, Tubular proteinuria in mice and humans lacking the intrinsic lysosomal protein SCARB2/Limp-2, Am. J. Physiol. Renal Physiol. 300 (2011) F1437–F1447.

[20] G. Rubboli, S. Franceschetti, S.F. Berkovic, L. Canafoglia, A. Gambardella, L. M. Dibbens, P. Riguzzi, C. Campieri, A. Magaudda, C.A. Tassinari, R. Michelucci, Clinical and neurophysiologic features of progressive myoclonus epilepsy without renal failure caused by SCARB2 mutations, Epilepsia 52 (2011) 2356–2363.

[21] P. Saftig, J. Klumperman, Lysosome biogenesis and lysosomal membrane proteins: trafficking meets function, Nat. Rev. Mol. Cell Biol. 10 (2009) 623–635.

[22] S. Ogata, M. Fukuda, Lysosomal targeting of Limp II membrane glycoprotein requires a novel Leu-Ile motif at a particular position in its cytoplasmic tail, J. Biol. Chem. 269 (1994) 5210–5217.

[23] I.V. Sandoval, J.J. Arredondo, J. Alcalde, A. Gonzalez Noriega, J. Vandekerckhove, M.A. Jimenez, M. Rico, The residues Leu(Ile)475-Ile(Leu, Val, Ala)476, contained in the extended carboxyl cytoplasmic tail, are critical for targeting of the resident lysosomal membrane protein LIMP II to lysosomes, J. Biol. Chem. 269 (1994) 6622–6631.

[24] M.A. Vega, F. Rodriguez, B. Seguí, C. Calés, J. Alcalde, I.V. Sandoval, Targeting of lysosomal integral membrane protein LIMP II. The tyrosine-lacking carboxyl cytoplasmic tail of LIMP II is sufficient for direct targeting to lysosomes, J. Biol. Chem. 266 (1991) 16269–16272.

[25] D. Neculai, M. Schwake, M. Ravichandran, F. Zunke, R.F. Collins, J. Peters, M. Neculai, J. Plumb, P. Loppnau, J.C. Pizarro, A. Seitova, W.S. Trimble, P. Saftig, S. Grinstein, S. Dhe-Paganon, Structure of LIMP-2 provides functional insights with implications for SR-BI and CD36, Nature 504 (2013) 172–176.

[26] J. Blanz, J. Groth, C. Zachos, C. Wehling, P. Saftig, M. Schwake, Disease-causing mutations within the lysosomal integral membrane protein type 2 (LIMP-2) reveal the nature of binding to its ligand β-glucocerebrosidase, Hum. Mol. Genet. 19 (2010) 563–572.

[27] F. Zunke, L. Andresen, S. Wesseler, J. Groth, P. Arnold, M. Rothaug, J.R. Mazzulli, D. Krainc, J. Blanz, P. Saftig, M. Schwake, Characterization of the complex formed by β-glucocerebrosidase and the lysosomal integral membrane protein type-2, Proc. Natl. Acad. Sci. U. S. A. (2016).

[28] C. Zachos, J. Blanz, P. Saftig, M. Schwake, A critical histidine residue within LIMP-2 mediates pH sensitive binding to its ligand β-glucocerebrosidase, Traffic 13 (2012) 1113–1123.

[29] M. Rothaug, F. Zunke, J.R. Mazzulli, M. Schweizer, H. Altmeppen, R. Lullmann-Rauch, W.W. Kallemeijn, P. Gaspar, J.M. Aerts, M. Glatzel, P. Saftig, D. Krainc, M. Schwake, J. Blanz, LIMP-2 expression is critical for β-glucocerebrosidase activity and -synuclein clearance, Proc. Natl. Acad. Sci. 111 (2014) 15573–15578.

[30] P. Gaspar, W.W. Kallemeijn, A. Strijland, S. Scheij, M. Van Eijk, J. Aten, H. S. Overkleeft, A. Balreira, F. Zunke, M. Schwake, C. Sá Miranda, J.M.F.G. Aerts,

Action myoclonus-renal failure syndrome: diagnostic applications of activity-based probes and lipid analysis, J. Lipid Res. 55 (2014) 138–145.
[31] M.J. Ferraz, W.W. Kallemeijn, M. Mirzaian, D. Herrera Moro, A. Marques, P. Wisse, R.G. Boot, L.I. Willems, H.S. Overkleeft, J.M. Aerts, Gaucher disease and Fabry disease: new markers and insights in pathophysiology for two distinct glycosphingolipidoses, Biochim. Biophys. Acta 1841 (2014) 811–825.
[32] K.S. Conrad, T.W. Cheng, D. Ysselstein, S. Heybrock, L.R. Hoth, B.A. Chrunyk, C. W. Am Ende, D. Krainc, M. Schwake, P. Saftig, S. Liu, X. Qiu, M.D. Ehlers, Lysosomal integral membrane protein-2 as a phospholipid receptor revealed by biophysical and cellular studies, Nat. Commun. 8 (2017) 1908.
[33] S. Heybrock, K. Kanerva, Y. Meng, C. Ing, A. Liang, Z.J. Xiong, X. Weng, Y. Ah Kim, R. Collins, W. Trimble, R. Pomes, G.G. Prive, W. Annaert, M. Schwake, J. Heeren, R. Lullmann-Rauch, S. Grinstein, E. Ikonen, P. Saftig, D. Neculai, Lysosomal integral membrane protein-2 (LIMP-2/SCARB2) is involved in lysosomal cholesterol export, Nat. Commun. 10 (2019) 3521.
[34] Y. Meng, S. Heybrock, D. Neculai, P. Saftig, Cholesterol handling in lysosomes and beyond, Trends Cell Biol. 30 (2020) 452–466, 781.
[35] J.P. Dobert, J.H. Schäfer, T. Dal Maso, P. Ravindran, D.J.E. Huard, E. Socher, L. A. Schildmeyer, R.L. Lieberman, W. Versées, A. Moeller, F. Zunke, P. Arnold, Cryo-TEM structure of β-glucocerebrosidase in complex with its its transporter LIMP-2, Nat. Commun. 16 (1) (2025) 3074, https://doi.org/10.1038/s41467-025-58340-1. PMID: 40159502; PMCID: PMC11955523. Mar 30.
[36] J. Zheng, L. Chen, O.S. Skinner, D. Ysselstein, J. Remis, P. Lansbury, R. Skerlj, M. Mrosek, U. Heunisch, S. Krapp, J. Charrow, M. Schwake, N.L. Kelleher, R. B. Silverman, D. Krainc, B-Glucocerebrosidase modulators promote dimerization of β-Glucocerebrosidase and reveal an allosteric binding site, J. Am. Chem. Soc. 140 (18) (2018) 5914–5924, https://doi.org/10.1021/jacs.7b13003. PMID: 29676907; PMCID: PMC6098685.
[37] S. Rudnik, S. Heybrock, E. Coyaud, Z. Xu, D. Neculai, B. Raught, V. Oorschot, C. Heus, J. Klumperman, P. Saftig, The lysosomal lipid transporter LIMP-2 is part of lysosome-ER STARD3-VAPB-dependent contact sites, J. Cell Sci. 137 (22) (2024) jcs261810, https://doi.org/10.1242/jcs.261810. Nov 15. (PMID: 39370902).
[38] J.P. Dobert, S. Bub, R. Mächtel, D. Januliene, L. Steger, M. Regensburger, S. Wilfling, J.X. Chen, M. Dejung, S. Plötz, U. Hehr, A. Moeller, P. Arnold, F. Zunke, Activation and purification of ß-glucocerebrosidase by exploiting its transporter LIM–-2 - implications for novel treatment strategies in Gau'her's and Parki'son's disease, Adv. Sci. (Weinh.). 11 (25) (2024 Jul) e2401641, https://doi.org/10.1002/advs.202401641. PMID: 38666485; PMCID: PMC11220700.
[39] D. Pietrafesa, A. Casamassa, B. Benassi, M. Santoro, M. Marano, C. Consales, J. Rosati, C. Arcangeli, Investigating the impact of the Parki'son's-associated GBA1 E326K mutation on β-glucocerebrosidase dimerization and interactome dynamics through an in silico approach, Int. J. Mol. Sci. 25 (21) (2024) 11443, https://doi.org/10.3390/ijms252111443. PMID: 39518995; PMCID: PMC11870034. Oct 24.
[40] A.-C. Gamp, Y. Tanaka, R. Lullmann-Rauch, D. Wittke, R. D'Hooge, P.P. De Deyn, T. Moser, H. Maier, D. Hartmann, K. Reiss, A.-L. Illert, K. von Figura, P. Saftig, LIMP-2/LGP85 deficiency causes ureteric pelvic junction obstruction, deafness and peripheral neuropathy in mice, Hum. Mol. Genet. 12 (2003) 631–646.
[41] M.D. Witte, W.W. Kallemeijn, J. Aten, K.-Y. Li, A. Strijland, W.E. Donker-Koopman, A.M.C.H. van den Nieuwendijk, B. Bleijlevens, G. Kramer, B.I. Florea, B. Hooibrink, C.E.M. Hollak, R. Ottenhoff, R.G. Boot, G. a van der Marel, H.S. Overkleeft, J.M.F. G. Aerts, Ultrasensitive in situ visualization of active glucocerebrosidase molecules, Nat. Chem. Biol. 6 (2010) 907–913.
[42] W.W. Kallemeijn, M.D. Witte, T.M. Voorn-Brouwer, M.T.C. Walvoort, K.-Y. Li, J.D. C. Codée, G.A. van der Marel, R.G. Boot, H.S. Overkleeft, J.M.F.G. Aerts, A sensitive gel-based method combining distinct cyclophellitol-based probes for the identification of acid/base residues in human retaining β-glucosidases, J. Biol. Chem. 289 (2014) 35351–35362.
[43] N. Dekker, L. van Dussen, C.E.M. Hollak, H. Overkleeft, S. Scheij, K. Ghauharali, M. J. van Breemen, M.J. Ferraz, J.E.M. Groener, M. Maas, F.A. Wijburg, D. Speijer, A. Tylki-Szymanska, P.K. Mistry, R.G. Boot, J.M. Aerts, Elevated plasma glucosylsphingosine in Gaucher disease: relation to phenotype, storage cell markers, and therapeutic response, Blood 118 (2011) e118–e127.
[44] M.J. Ferraz, A.R.A. Marques, M.D. Appelman, M. Verhoek, A. Strijland, M. Mirzaian, S. Scheij, C.M. Ouairy, D. Lahav, P. Wisse, H.S. Overkleeft, R.G. Boot, J.M. Aerts, Lysosomal glycosphingolipid catabolism by acid ceramidase: formation of glycosphingoid bases during deficiency of glycosidases, FEBS Lett. 590 (2016) 716–725.
[45] A.R.A. Marques, M. Mirzaian, H. Akiyama, P. Wisse, M.J. Ferraz, P. Gaspar, K. Ghauharali-van der Vlugt, R. Meijer, P. Giraldo, P. Alfonso, P. Irún, M. Dahl, S. Karlsson, E.V. Pavlova, T.M. Cox, S. Scheij, M. Verhoek, R. Ottenhoff, C.P.A. A. van Roomen, N.S. Pannu, M. van Eijk, N. Dekker, R.G. Boot, H.S. Overkleeft, E. Blommaart, Y. Hirabayashi, J.M. Aerts, Glucosylated cholesterol in mammalian cells and tissues: formation and degradation by multiple cellular β-glucosidases, J. Lipid Res. 57 (2016) 451–463.
[46] M. Damme, W. Morelle, B. Schmidt, C. Andersson, J. Fogh, J.-C. Michalski, T. Lübke, Impaired lysosomal trimming of N-linked oligosaccharides leads to hyperglycosylation of native lysosomal proteins in mice with -mannosidosis, Mol. Cell. Biol. 30 (2010) 273–283.
[47] G. Kramer, Y. Woolerton, J.P. van Straalen, J.P.C. Vissers, N. Dekker, J. I. Langridge, R.J. Beynon, D. Speijer, A. Sturk, J.M.F.G. Aerts, Accuracy and reproducibility in quantification of plasma protein concentrations by mass spectrometry without the use of isotopic standards, PloS One 10 (2015) e0140097.
[48] J.M. Aerts, W.E. Donker-Koopman, M.K. van der Vliet, L.M. Jonsson, E.I. Ginns, G. J. Murray, J.A. Barranger, J.M. Tager, A.W. Schram, The occurrence of two immunologically distinguishable β-glucocerebrosidases in human spleen, Eur. J. Biochem. 150 (1985) 565–574.
[49] J.E.M. Groener, B.J.H.M. Poorthuis, S. Kuiper, M.T.J. Helmond, C.E.M. Hollak, J. M.F.G. Aerts, HPLC for simultaneous quantification of total ceramide, glucosylceramide, and ceramide trihexoside concentrations in plasma, Clin. Chem. 53 (2007) 742–747.
[50] M. Mirzaian, P. Wisse, M.J. Ferraz, H. Gold, W.E. Donker-Koopman, M. Verhoek, H. S. Overkleeft, R.G. Boot, G. Kramer, N. Dekker, J.M.F.G. Aerts, Mass spectrometric quantification of glucosylsphingosine in plasma and urine of type 1 Gaucher patients using an isotope standard, Blood Cells Mol. Dis. 54 (2015) 307–314.
[51] J. Folch, M. Lees, G.H. Sloane Stanley, A simple method for the isolation and purification of total lipides from animal tissues, J. Biol. Chem. 226 (1957) 497–509.
[52] M. Mirzaian, G. Kramer, B.J.H.M. Poorthuis, Quantification of sulfatides and lysosulfatides in tissues and body fluids by liquid chromatography-tandem mass spectrometry, J. Lipid Res. 56 (2015) 936–943.
[53] A.R.A. Marques, J. Aten, R. Ottenhoff, C.P.a.a. van Roomen, D. Herrera Moro, N. Claessen, M.F. Vinueza Veloz, K. Zhou, Z. Lin, M. Mirzaian, R.G. Boot, C.I. De Zeeuw, H.S. Overkleeft, Y. Yildiz, J.M.F.G. Aerts, Reducing GBA2 activity ameliorates neuropathology in Niemann-pick type C mice, PLoS One 10 (2015) e0135889.
[54] A.R. Marques, T.L. Gabriel, J. Aten, C.P. van Roomen, R. Ottenhoff, N. Claessen, P. Alfonso, P. Irún, P. Giraldo, J.M. Aerts, M. van Eijk, Gpnmb is a potential marker for the visceral pathology in Niemann-Pick type C disease, PLoS One 11 (1) (2016) e0147208. Jan 15.
[56] M. Dahl, A. Doyle, K. Olsson, J.-E. Månsson, A.R.A. Marques, M. Mirzaian, J. M. Aerts, M. Ehinger, M. Rothe, U. Modlich, A. Schambach, S. Karlsson, Lentiviral gene therapy using cellular promoters cures type 1 Gaucher disease in mice, Mol. Ther. 23 (2015) 835–844.
[57] P.K. Mistry, J. Liu, M. Yang, T. Nottoli, J. McGrath, D. Jain, K. Zhang, J. Keutzer, W.-L. Chuang, W.Z. Mehal, H. Zhao, A. Lin, S. Mane, X. Liu, Y.Z. Peng, J.H. Li, M. Agrawal, L.-L. Zhu, H.C. Blair, L.J. Robinson, J. Iqbal, L. Sun, M. Zaidi, Glucocerebrosidase gene-deficient mouse recapitulates Gaucher disease displaying cellular and molecular dysregulation beyond the macrophage, Proc. Natl. Acad. Sci. U. S. A. 107 (2010) 19473–19478.
[59] M. Siebert, E. Sidransky, W. Westbroek, Glucocerebrosidase is shaking up the synucleinopathies, Brain 137 (2014) 1304–1322.
[60] H. Michelakakis, G. Xiromerisiou, E. Dardiotis, M. Bozi, D. Vassilatis, P.-M. Kountra, G. Patramani, M. Moraitou, D. Papadimitriou, E. Stamboulis, L. Stefanis, E. Zintzaras, G.M. Hadjigeorgiou, Evidence of an association between the scavenger receptor class B member 2 gene and Parkinson's disease, Mov. Disord. 27 (2012) 400–405.
[61] E. Maniwang, N. Tayebi, E. Sidransky, Is Parkinson disease associated with lysosomal integral membrane protein type-2?: challenges in interpreting association data, Mol. Genet. Metab. 108 (2013) 269–271.
[62] R. Thomas, E.B. Moloney, Z.K. Macbain, P.J. Hallett, O. Isacson, Fibroblasts from idiopathic Parki'son's disease exhibit deficiency of lysosomal glucocerebrosidase activity associated with reduced levels of the trafficking receptor LIMP2, Mol. Brain 14 (1) (2021) 16, https://doi.org/10.1186/s13041-020-00712-3. PMID: 33468204; PMCID: PMC7816505.
[63] Y.W. Zhao, H.X. Pan, Z. Liu, Y. Wang, Q. Zeng, Z.H. Fang, T.F. Luo, K. Xu, Z. Wang, X. Zhou, R. He, B. Li, G. Zhao, Q. Xu, Q.Y. Sun, X.X. Yan, J.Q. Tan, J.C. Li, J.F. Guo, B.S. Tang, The association between lysosomal storage disorder genes and Parki'son's disease: a large cohort study in Chinese mainland population, Front. Aging Neurosci. 13 (2021) 749109, https://doi.org/10.3389/fnagi.2021.749109. Nov 15. PMID: 34867278; PMCID: PMC8634711.
[64] M. Yu, H. Ye, R.B. De-Paula, C.G. Mangleburg, T. Wu, T.V. Lee, Y. Li, D. Duong, B. Phillips, C. Cruchaga, G.I. Allen, N.T. Seyfried, I. Al-Ramahi, J. Botas, J. M. Shulman, Functional screening of lysosomal storage disorder genes identifies modifiers of alpha-synuclein neurotoxicity, PLoS Genet. 19 (5) (2023) e1010760, https://doi.org/10.1371/journal.pgen.1010760. PMID: 37200393; PMCID: PMC10231792.
[65] P. García-Sanz, J. M F G Aerts, R. Moratalla, The role of cholesterol in α-synuclein and Lewy body pathology in GBA1 Parkinson's disease, Mov. Disord. 36 (5) (2021 May) 1070–1085, https://doi.org/10.1002/mds.28396 (PMID: 33219714; PMCID: PMC8247417).
[66] A.M. Petrov, M.R. Kasimov, A.L. Zefirov, Cholesterol in the pathogenesis of Alzheimer's, Parkinson's diseases and autism: link to synaptic dysfunction, Acta Nat. 9 (1) (2017 Jan–Mar) 26–37 (PMID: 28461971; PMCID: PMC5406657).